Hierarchical approach towards adsorptive removal of Alizarin Red S dye using native chitosan and its successively modified versions

M. A. Khapre and R. M. Jugade

ABSTRACT

In the present work, native chitosan (Ch) along with its chemically and physico-chemically modified versions, namely sulphate cross-linked chitosan (SCC) and sulphate cross-linked chitosan–bentonite composite (SCC-B), were employed as potential adsorbents for the removal of an anionic dye, Alizarin Red S (ARS) from aqueous solutions. All three adsorbents were extensively characterized using techniques such as Fourier-transform infrared spectroscopy, scanning electron microscopy, energy dispersive X-ray, X-ray diffraction, Brunauer–Emmett–Teller analysis, thermogravimetric–differential thermal analysis, and pH point of zero charge. Various parameters were optimized, including pH of dye solution, contact time, adsorbent dose, initial adsorbate concentration and temperature of adsorption. Four adsorption isotherm models were studied and it was found that the Freundlich model was best-fit for all three systems. Maximum adsorption capacities towards adsorption of ARS were found to be 42.48, 109.12 and 131.58 mg g^{-1} for Ch, SCC and SCC-B, respectively. Kinetics of adsorption was examined by employing three well-known models in order to deduce the mechanism of adsorption. Thermodynamic studies show that the process is spontaneous and exothermic for all adsorbents employed. Furthermore, it was observed that for large sample volumes, the column adsorption method was more effective compared to the batch method.

Key words | adsorption, adsorption isotherms, Alizarin Red S, chitosan, kinetics, thermodynamics

M. A. Khapre (corresponding author)
R. M. Jugade
PG Department of Chemistry,
RTM Nagpur University,
Nagpur 440 033, Maharashtra,
India
E-mail: *mkhapre195@gmail.com*

HIGHLIGHTS

- Native chitosan (Ch), sulphate cross-linked chitosan (SCC) and sulphate cross-linked chitosan-bentonite composite (SCC-B) were employed as potential adsorbents for removal of Alizarine Red S dye (ARS).
- All three adsorbents were subjected to intense characterization using various spectral techniques such as Fourier-transform infrared spectroscopy, scanning electron microscopy, energy dispersive X-ray, X-ray diffraction, Brunauer–Emmett–Teller analysis, and thermogravimetric-differential thermal analysis.
- The applicability of four different adsorption isotherm models was checked for all three adsorbents. These include Langmuir, Freundlich, Halsey and Redlich–Peterson (R–P) models.
- The maximum removal efficiency was found to be highest for SCC-B followed by SCC and Ch.
- Adsorption kinetics, thermodynamics and column studies for all the three adsorbate–adsorbent systems were also performed.

doi: 10.2166/wst.2020.376

GRAPHICAL ABSTRACT

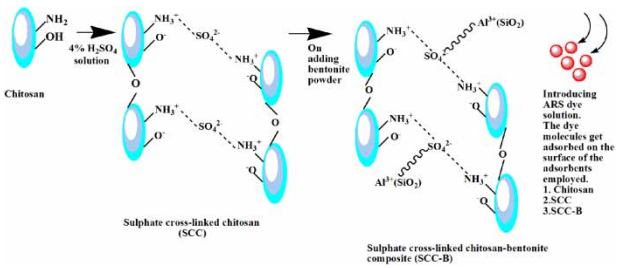

INTRODUCTION

Dyes are inevitable constituents of many industries like textile, paper, rubber, leather, plastics, etc. and their presence in wastewater is a matter of great concern to environmentalists (Ho & Ching 2001). Many of the dyes are stable to light, oxidation and even resistant to aerobic digestion (Chen & Zhao 2009). Removal of dyes from water has been a major challenge and a number of methods have been adopted for this purpose, such as membrane filtration, photodegradation (Naushad *et al.* 2019), coagulation–flocculation, biological treatment, electro-chemical process and adsorption (Huang *et al.* 2015).

Adsorption (Vital *et al.* 2016), among all the other methods available, has been found to be highly useful because it is cost effective, simple, quick and applicable to large-scale effluents (Jeyaseelan *et al.* 2018). A variety of adsorbent materials are currently available, which include low-cost materials (Crini 2006; Bharathi & Ramesh 2013) such as alum sludge (Tripathy *et al.* 2006), clays (Fu *et al.* 2011; Komosińska *et al.* 2014; Adeyemo *et al.* 2017), chitosan (Ch) (Chatterjee *et al.* 2007; Saha *et al.* 2010; Kyzas & Bikiaris 2015), bio-composite (Nair *et al.* 2014; Saravanan *et al.* 2013; Dotto *et al.* 2016) and agricultural waste (Namasivayam & Kavitha 2002; Singh *et al.* 2003; Adekola & Adegoke 2005; Bulut & Aydin 2006; Mahmoodi *et al.* 2011; Salleh *et al.* 2011). Among these materials, bio-composites have attracted great attention because of their high adsorption capacities and good mechanical strength.

Ch, a well-known biopolymer, is obtained by deacetylation of chitin, which is a component of crustacean shells as well as fungal biomass. It has a wide range of applications in fields like food, cosmetics, medicine and pharmaceuticals. It is biodegradable, biocompatible and its degradation products are non-toxic. Due to its chemical stability, high reactivity and good chelation property, it can be used for the removal of dyes (Vital *et al.* 2016). Ch still has some disadvantages, including poor mechanical strength, easy agglomeration and its solubility in dilute acids. However, Ch is insoluble in sulphuric acid. The free amino groups react with acid to form salt, and because sulphuric acid is divalent, cross-linking occurs thus providing the necessary mechanical strength to the polymer chain. Kahu *et al.* has reported the synthesis of sulphate cross-linked chitosan (SCC) and its application in the removal of hexavalent chromium (Kahu *et al.* 2014).

Clay materials are generally made up of hydrous alumina-silicates, with high cation exchange capacity and large specific surface area. Furthermore, clay minerals are abundant in nature, cheaply available and mechanically stable making it an attractive immobilization material for Ch (Nesic *et al.* 2013). Among the mineral clays, bentonite has been highlighted for the preparation of composites because of its high cationic exchange capacity and the possibility of lamellar expansion (Anirudhan *et al.* 2010). Bentonite has proven to be a promising economic material for the removal of dyes due to its large abundance (Bellir *et al.* 2010).

In the present work, native Ch, cross-linked CH and Ch–bentonite composite have been employed as potential adsorbents for the removal of an anionic dye – Alizarin Red S (ARS). It is an organic sodium dye, commonly known as sodium alizarinsulphonate (Supplementary Figure 1). The molecular formula is $C_{14}H_7NaO_7S$ and molecular weight is 342.253 g/mol. ARS is widely used in textile industries to impart colour to the fabrics, but it is known to cause skin, eye and respiratory tract irritation when exposed for a long duration.

MATERIALS AND METHOD

Materials

Ch powder-652 (high density) was supplied by Meck Pharmaceuticals & Chemicals Pvt. Ltd, Ahmadabad, India. Sulphuric acid AR (98%) was supplied by SDFCL, Mumbai, India. Bentonite powder and Alizarin Red S AR (sodium alizarin sulphonate) were supplied by Loba Chemie Pvt. Ltd, Mumbai. Aqueous solutions were prepared using double distilled water. All reagents used were of analytical grade and no further purification was done.

Preparation of sulphate cross-linked chitosan-bentonite composite (SCC-B)

Kahu *et al.* (2014) described in detail the preparation of SCC. It involves treating 5.0 g Ch with 250 mL 4% (v/v) sulphuric acid solution in a round-bottom flask and stirring for 1 h at room temperature. Resultant SCC was filtered and washed until the washings had a neutral pH. In order to prepare sulphate cross-linked chitosan–bentonite composite (SCC-B), 5.0 g of bentonite powder was added to the Ch–sulphuric acid solution after 1 h of stirring and was then stirred continuously for the next 12 h using a magnetic stirrer. The mixture was then filtered and the material washed several times with double-distilled water until the washings were completely free from acidity. It was dried in a hot air oven for 12 h at 50 °C, crushed using a mortar and pestle and sieved through 350 micron mesh a to obtain uniform particle size. The material obtained was SCC-B and was used as an adsorbent for ARS.

pH_{PZC} of adsorbent materials

The pH point of zero charge (pH_{PZC}) is the pH value at which the net charge on the surface of the adsorbent material is zero (Jeyaseelan *et al.* 2018). The net charge on the adsorbent surface is positive below this pH, but is negative above this pH. Hence the value of pH_{PZC} can be used for the prediction of adsorbent–adsorbate interaction. For determining pH_{PZC}, 25 mL of 0.01M sodium chloride solution was taken in conical flask. The initial pH values were adjusted between 2.0 to 10.0 using dilute solutions of hydrochloric acid and sodium hydroxide. To each of the flasks, 0.1 g of the adsorbent was added, stirred for 24 h and the final pH values were noted after filtration. The values of pH_{PZC} were determined from the plot of change in pH as a function of initial pH.

Batch adsorption experiments

For performing batch experiments, 50 mL dye solution (of known concentration) was equilibrated with a known amount of adsorbent (Ch, SCC or SCC-B) in a stoppered conical flask. Adsorption systems were stirred on a mechanical shaking machine at 170 rpm for the desired time at room temperature. The systems were then filtered and the absorbance value of the filtrate was recorded. Filter paper itself was found to adsorb some dye leading to decrease of about 0.4% in the absorbance value. This correction was applied in all the calculations. The absorption maxima (λ_{max}) and absorbance values were recorded using Equiptronics EQ-824 dual beam spectrophotometer in the range 350–1,100 nm using a set of matched cuvettes. The pH was adjusted using Equiptronics pH meter EQ-615. For uniform stirring of the dye solution with the adsorbents, a Remi RS-12R DX mechanical shaking machine was used (range 80–180 rpm).

The quantity of dye adsorbed per gram of adsorbent at equilibrium (q_e) can be calculated as follows:

$$q_e = (C_o - C_e) \times V/W \quad (1)$$

where C_o and C_e indicate the initial and equilibrium liquid phase concentration (mg L^{-1}) of the dye, V is the volume of dye solution in litres and W is the weight of adsorbent in grams. All batch experiments were performed in three replicates and average values were reported to obtain reliable results.

Column adsorption experiments

The column studies were carried out using 50 mg L^{-1} ARS solution. A glass column was packed with 1.0 g of the adsorbent material (Ch, SCC or SCC-B). ARS solution with desired pH was eluted from the column at an optimized flow rate of 5 mL min^{-1}. Effluent from the column was collected at every 10 min intervals and analyzed spectrophotometrically until the outlet concentrations reached an equilibrium value. The breakthrough capacity, exhaustion capacity and column efficiency were calculated using

following equations:

$$\text{Breakthrough capacity (mg g}^{-1}) = \frac{\text{Breakthrough volume (L)} \times \text{Inlet dye concentration (ppm)}}{\text{Weight of adsorbent(g)}} \quad (2)$$

$$\text{Exhaustion capacity (mg g}^{-1}) = \frac{\text{Exhaustion volume (L)} \times \text{Inlet dye concentration (ppm)}}{\text{Weight of adsorbent (g)}} \quad (3)$$

$$\text{Column efficiency (\%)} = \frac{\text{Breakthrough volume (L)}}{\text{Exhaustion volume (L)}} \times 100 \quad (4)$$

Characterization of the synthesized biopolymer

Characterization was carried out by subjecting the adsorbents using Fourier-transform infrared spectroscopy (FT-IR), scanning electron microscopy (SEM), energy dispersive X-ray (EDX), X-ray diffraction (XRD), thermogravimetric-differential thermal analysis (TGA–DTA), and Brunauer–Emmett–Teller (BET) analysis surface area analysis. FT-IR spectra were recorded using a Bruker Alpha spectrometer in the range of 500 to 4,000 cm^{-1}. Surface morphology of adsorbents was studied using and SEM model TESCAN VEGA 3 SBH. EDX spectroscopy for elemental analysis was obtained using an X-ray analyser Oxford INCA Energy 250 EDS System during SEM analysis. The XRD spectra were recorded using an X-ray diffractometer system Rigaku-Miniflex 300. The TGA–DTA analysis was carried out using Shimadzu DTG-60 simultaneous DTA–TG apparatus. The BET surface area analysis was carried out using a Surface Area Analyzer Model-SmartSorb 92/93.

RESULTS AND DISCUSSION

FT-IR spectral characterization

The FT-IR spectrum of Ch (Figure 1(a)) shows characteristic broad peaks corresponding to O–H and N–H stretching vibrations in the region 3,300 $cm^{-1}$and 3,500 cm^{-1}, respectively (Savitri & Budhyantaro 2017; Jeyaseelan *et al.* 2018). The N–H bending vibrations were observed around 1,540 cm^{-1}. The C–H and the C–O stretching bands were obtained around 2,790 cm^{-1} and 1,020 cm^{-1}, respectively. The FT-IR spectrum of SCC (Figure 1(b)) also shows the characteristic broad peaks that are analogous to that of Ch. Sharp peaks were found around 580–640 cm^{-1}, which corresponds to the presence of a sulphate group (Kahu *et al.* 2014; Jeyaseelan *et al.* 2018). In the FT-IR spectrum of SCC-B (Figure 1(c)), the region below 600 cm^{-1} corresponds to the presence of quartz, i.e. Si–O–Si bonds. The bands appearing in the region around 678 cm^{-1} refers to the presence of feldspar, i.e. Al–O–Si–O bonds, and those around 918 cm^{-1} indicates the presence of Al–Al–OH bonds. The appearance of bands around 1,650 cm^{-1} and 3,405 cm^{-1} refer to the presence of adsorbed water (Grozdanov *et al.* 2016).

After adsorption of ARS (Figure 1(d), 1(f) and 1(e)) on these materials, the characteristic peaks of ARS were observed around 1,670 cm^{-1}, corresponding to the C=O group (Holmgren *et al.* 1997). The peaks of $-NH_2$ group has also been found to shift towards a higher wave number, indicating an interaction with the ARS molecule.

SEM analysis

SEM micrographs (Figure 2) explore the surface morphology of the adsorbent material. The SEM image of pure Ch (Figure 2(a)) shows a degree of irregularity in the surface, as well as a denseness in the structure. After treatment with sulphuric acid (Figure 2(b)), a regular arrangement appears, with a smoothness and a rigidness in the structure that is maintained throughout. This may be due to the presence of cross-linking, which is responsible for the enhanced regularity and stability of the material. The SEM image of SCC-B (Figure 2(c)) shows the similar regularity and orderly structure with an illuminating layer above it. These bright areas are attributed to the alumina, silica and quartz groups present in the bentonite powder.

EDX analysis

EDX spectrum of Ch (Figure 3(a)) clearly shows the peaks of three major components of Ch – carbon, nitrogen and oxygen. A peak of sulphur is clearly visible in the spectrum of SCC (Figure 3(b)), which confirms the cross-linking effect. The EDX spectrum of SCC-B (Figure 3(c)) shows the peaks of aluminium, silicon and sulphur along with that of carbon, nitrogen and oxygen, which indicates the formation of SCC-bentonite composite.

XRD studies

In the XRD pattern (Figure 4), the characteristic diffraction peaks of Ch (Figure 4(a)) were observed at $2\theta = 10.94°$ and 21.8°, which are in accordance with the reported values

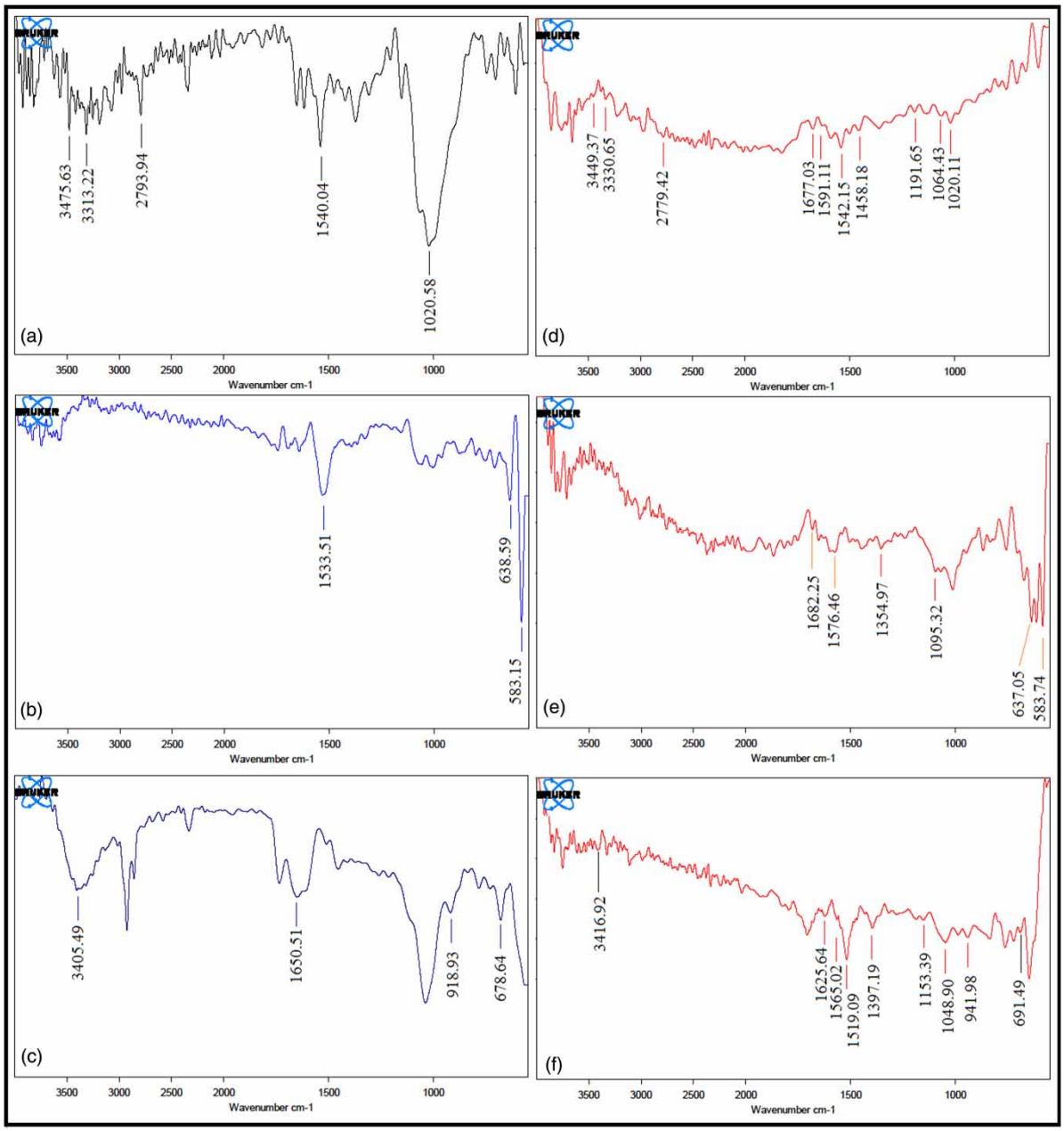

Figure 1 | FT-IR spectra of (a) Ch, (b) SCC and (c) SCC-B. FT-IR spectra of (d) Ch, (e) SCC and (f) SCC-B after adsorption of ARS.

(Kahu *et al.* 2014). The XRD spectra of SCC (Figure 4(b)) reveals the characteristic peaks at 2θ around 12.04° and 18.96°, which confirms the cross-linking effect of the sulphate group (Jeyaseelan *et al.* 2018). The peak at $2\theta =$ 23.27° refers to structural change in the Ch polymer due to the formation of a cross-linked chain (Shekhawat *et al.* 2015). In the case of SCC-B, the XRD analysis helps to determine whether Ch has entered into the interlayer spacing of bentonite (Savitri & Budhyantaro 2017). The XRD pattern of pure bentonite exhibits a typical peak of montmorillonite at $2\theta = 6.56°$. After interaction of bentonite with Ch, there was a slight shift of peak towards the lower diffraction angle, thus obtaining a peak at $2\theta = 5.94°$ (Figure 4(c)). This shift of peak may be attributed to a slight distortion of the intrinsic arrangement of the silicate layers and a decrease in the crystallinity of the molecule. These results confirm the incorporation of Ch into the interlayer spacing of bentonite (Huang *et al.* 2015). The peak at $2\theta = 19.3°$ is a characteristic

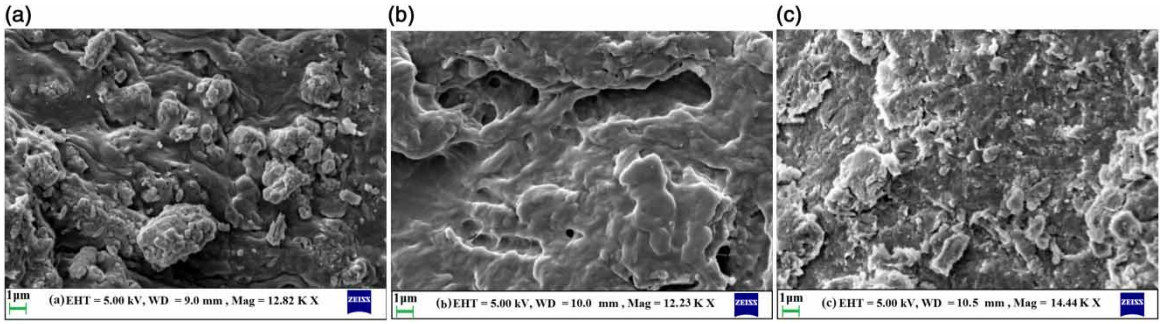

Figure 2 | SEM images of (a) Ch, (b) SCC and (c) SCC-B.

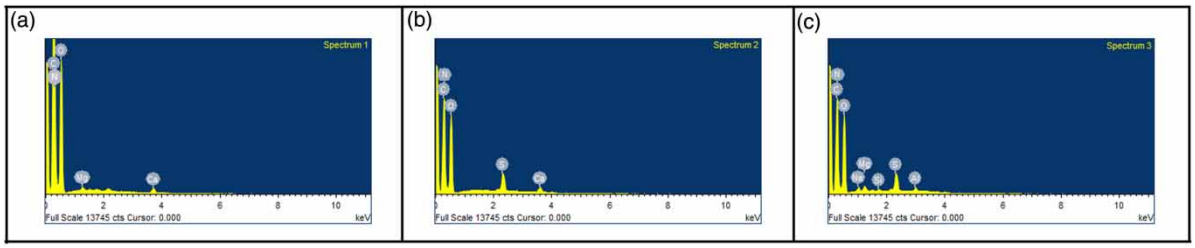

Figure 3 | EDX spectra of (a) Ch, (b) SCC and (c) SCC-B.

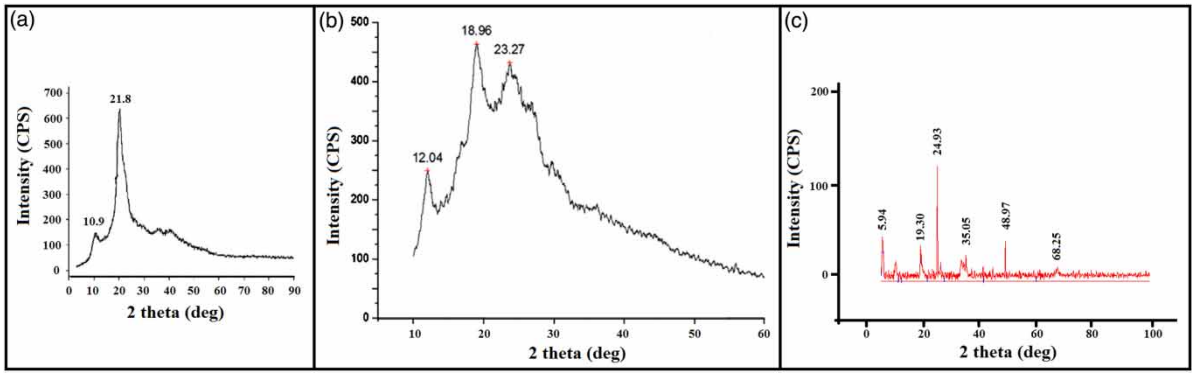

Figure 4 | XRD spectra of (a) Ch, (b) SCC and (c) SCC-B.

crystalline peak for the cross-linking phenomena (Huang *et al.* 2016), while the peak at $2\theta = 24.93°$ is relative to Ch (Dotto *et al.* 2016).

BET analysis

Surface area analysis was carried out using the nitrogen adsorption–desorption method. The surface area of Ch, SCC and SCC-B were found to be $3.47\ m^2\ g^{-1}$, $2.78\ m^2\ g^{-1}$ and SCC-B was $6.01\ m^2\ g^{-1}$. The decrease in surface area in SCC can be attributed to the cross-linking, leading to a reduction in cavities in the chitosan structure. The increase in surface area of SCC-B may be attributed to the binding of the bulky Si–O–Si groups and Al–O–Si–O groups to the surface of SCC. After adsorption of ARS, the surface area of each of the adsorbents was found to decrease. The surface area of chitosan and SCC were found to be below the detection limit of the instrument, while that of SCC-B was found to be $3.10\ m^2\ g^{-1}$. This clearly indicates surface coverage of the materials by the adsorbent.

Thermal analysis

Thermal analyses of samples were carried out to study the thermal stability and decomposition temperature of the

synthesized adsorbents. TGA–DTA analysis of Ch, SCC, SCC-B and pure bentonite was performed. The TGA curve of native Ch (Figure 5(a)) showed a two-step degradation, the first was around 50–100 °C, which corresponds to a loss of moisture, while the second degradation was at around 275 °C and continued up to 375 °C. The steep curve in this region indicates fast degradation, and above 400 °C the process slowed down with almost complete decomposition up to 1,000 °C. The DTA curve of Ch showed a strong and sharp exothermic peak at around 300 °C, which was attributed to its thermal decomposition. The TGA curve of SCC (Figure 5(b)) showed stepwise degradation, with a loss of moisture slowly up to 200 °C and two consecutive weight losses between 230 to 310 °C. The DTA curve shows two prominent endothermic peaks around 240 °C and 280 °C, respectively, which may be attributed to the degradation behaviour of the sulphate group and rearrangement reaction. In contrast to the exothermic peak obtained in the case of Ch, the SCC shows endothermic peaks, which indicate that SCC is less thermally stable due to the cross-linking effect of the sulphate group, which provides active sites for the uptake of dye molecules. Bentonite is thermally stable as an inorganic oxide and shows little degradation (Figure 5(c)), with a loss of moisture up to 100 °C and a loss of lattice water and removal of structural –OH groups at around 500 °C (Azzeddine & Abdelali 2014), with a small endothermic peak in the DTA curve. The TGA–DTA curves of SCC-B (Figure 5(d)) show characteristics of both SCC and bentonite. The degradation process involves a loss of moisture at around 100 °C. The composite prominently shows two endothermic peaks in the range 230–300 °C, which corresponds to the presence of SCC, and a small endothermic degradation around 500 °C, which corresponds to the presence of bentonite. This is a clear indication of the composite formation of the two materials.

Effect of pH

The pH of the dye solution is an important parameter that significantly affects the adsorption mechanism and the interaction between the dye molecules and the adsorbent, especially when the dye under consideration is an indicator dye. The pH of solution also affects the surface charge of the

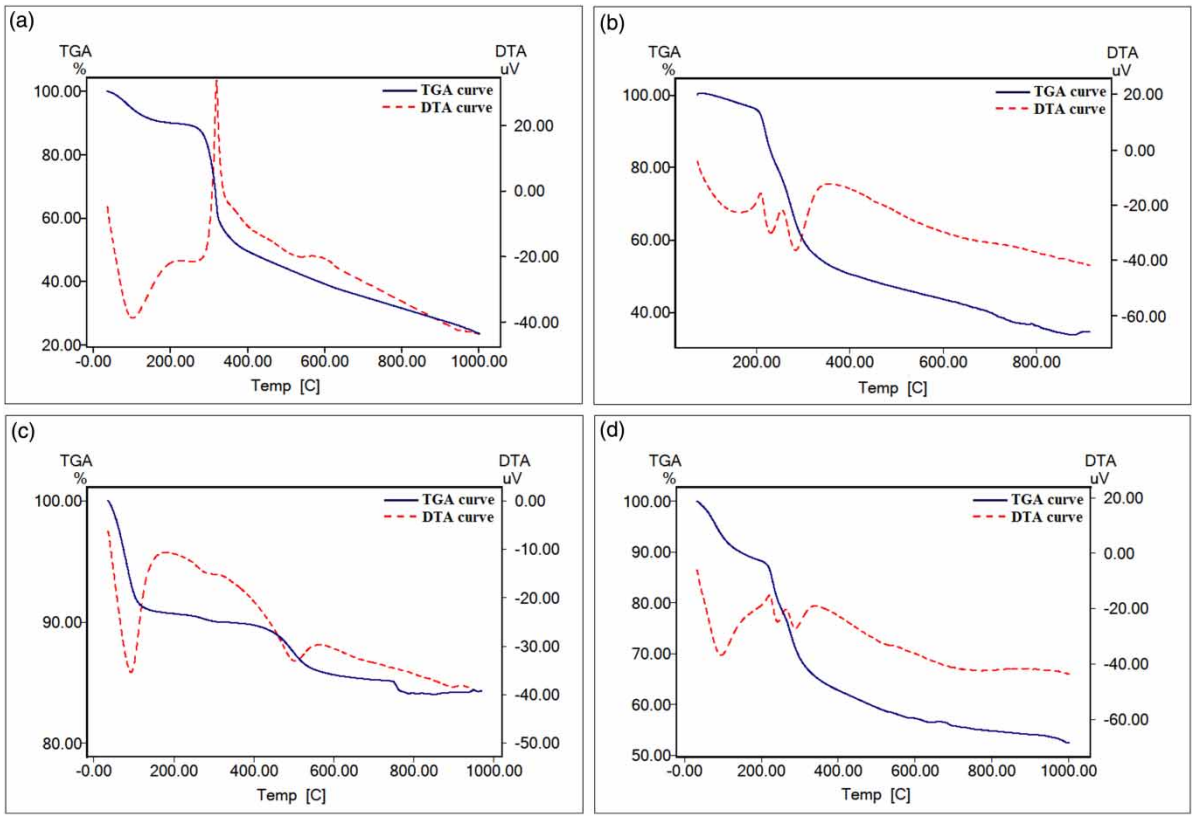

Figure 5 | TGA–DTA analysis of (a) Ch, (b) SCC, (c) bentonite and (d) SCC-B.

adsorbent. The pH_{PZC} values for Ch, SCC and SCC-B were found to be 8.2, 4.6 and 5.3, respectively (Figure 7(a)). The pH of the dye solutions (Figure 7(b)) varied from 2.0 to 9.0, and all other parameters were kept constant in order to determine the pH for maximum removal efficiency of the adsorbent. For Ch, the removal efficiency was highest at pH 3.0 because the adsorbent surface has a positive charge and the adsorption of anionic dye is favoured at pH less than pH_{PZC}. However, the decrease in adsorption from pH 4.0 onwards clearly indicates that the electrostatic attraction is not the only interaction between Ch and ARS. In SCC, the surface positive charges are linked with sulphate groups and hence the adsorption efficiency has a negligible effect of pH over a wide range (Kahu *et al.* 2014). For SCC-B, maximum adsorption occurred at pH 8.0, indicating that the particles of the clay-building mineral (bentonite) possess negative surface charge. It was impossible to bond the dye by means of the electrostatic interaction with the mineral surfaces. The dyes were mainly bonded with the hydrogen bonds, in which the –OH, –NH and $–NH_2$ groups acted as the proton donors and the –SiO and $–Al_2OH$ groups played the role of the proton acceptors. The studied dyes could also be bound due to the interactions of the hydrated interlayer Ca^{2+} ions. Similar observations have been reported for smectite clay (Kyzol-Komosińska *et al.* 2014). The proposed mechanism (Figure 6) for the uptake of ARS dye by Ch, SCC and SCC-B is depicted by the following scheme (Zhang *et al.* 2016).

The pH of 3.0 was selected for Ch, pH 8.0 was selected for SCC-B, but for SCC, the solution pH of dye (pH 6.5) was kept as it is. These pH conditions were used in all further studies.

Effect of contact time

The contact time (Figure 7(c)) of dye solution with adsorbent material was varied from 10 to 60 min. The optimum pH of the dye solution was set initially according to the type of adsorbent used, as discussed in the previous section. It was observed that, with an increase in contact time the adsorption efficiency of adsorbent increased, but the increase in adsorption became less significant later due to blocking of the available sites by the dye molecules. The equilibrium was attained at around 40 min for each adsorbent and hence the contact time of 40 min was fixed and further parameters were studied.

Effect of adsorbent dose

The adsorbent dose (Figure 7(d)) varied from 100 to 500 mg. It was observed that, with an increase in the amount of

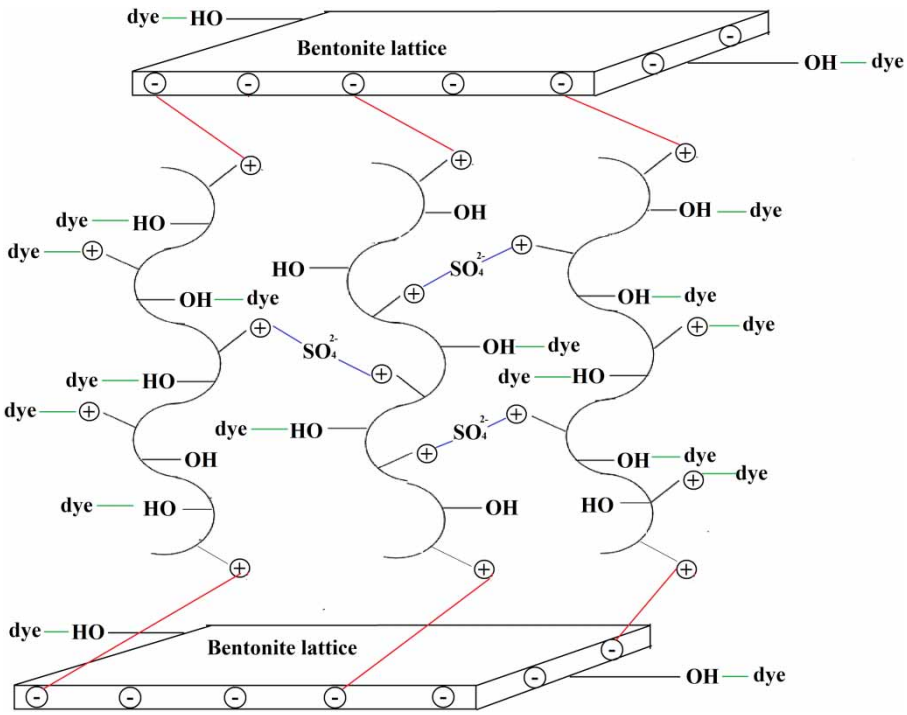

Figure 6 | Schematic diagram depicting the mechanism of uptake of ARS dye by Ch, SCC and SCC-B adsorbents.

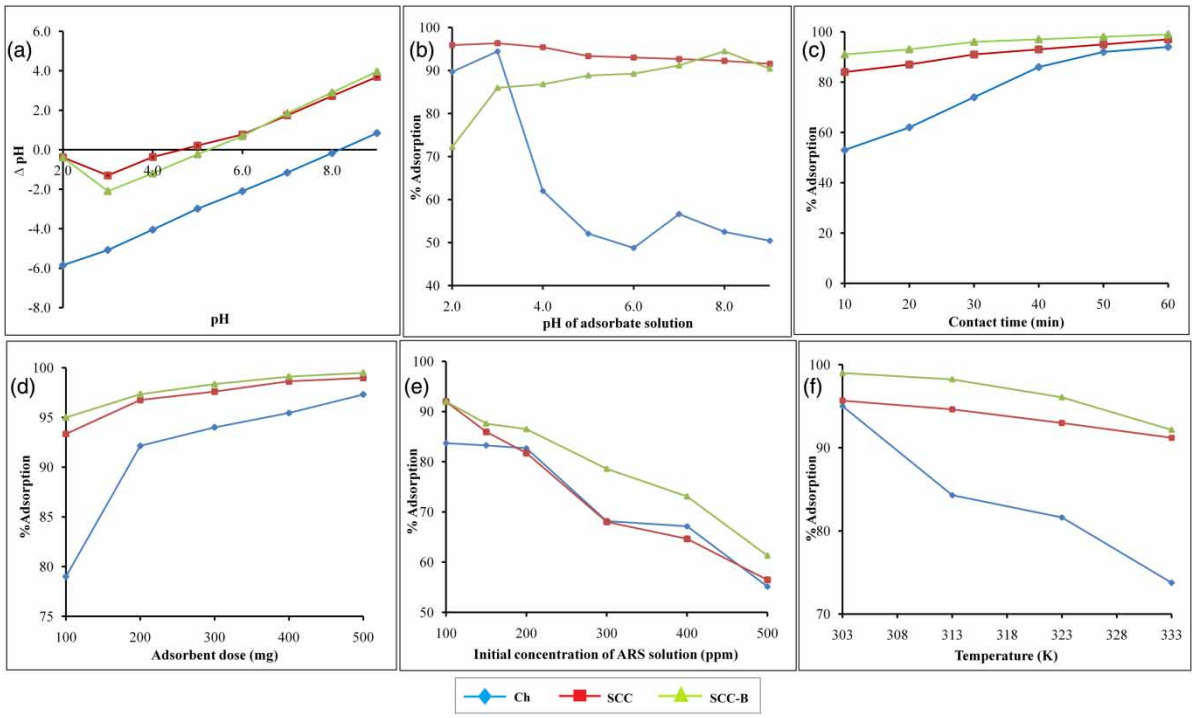

Figure 7 | Effect of operational parameters on adsorption efficiency.

adsorbent, efficiency of adsorption increased due to more availability of active sites on the surface of the adsorbent. For Ch, SCC and SCC-B, equilibrium adsorption was attained at 200 mg dose and hence it was optimized for the further studies.

Effect of concentration of adsorbate

The adsorption studies were carried out by varying the initial concentration (Figure 7(e)) of the dye solution from 50 to 500 mg L^{-1} for each of the adsorbents used and the optimized values of all other parameters. A steady decrease in the adsorption efficiency was observed with an increase in dye concentration for all the adsorbents used. This is due to the number of active sites on the surface of the adsorbent continuously being blocked by the incoming dye molecules and the number of sites becoming available is insufficient for the large number of dye molecules, and hence adsorption efficiency decreases.

Effect of temperature

Temperature studies (Figure 7(f)) were carried out by varying the temperature of the adsorbate–adsorbent system from 30 °C to 60 °C. There was a steady decrease in the adsorption efficiency with the rise in temperature from 30 °C to 60 °C for all three adsorbents studied. The results obtained were consistent with the observation that with an increase in temperature, adsorption decreases. Lower temperature favours adsorption, while higher temperature favours desorption.

Adsorption isotherms

Adsorption isotherms are essential in order to study the interaction between the adsorbate and adsorbent molecules. It describes the fraction of sorbate molecules that are partitioned between liquid and solid phases at equilibrium (Boparai *et al.* 2011). A number of adsorption isotherm models are available to understand the mechanism of adsorption, such as Langmuir, Freundlich, Redlich–Peterson, Halsey, Dubinin–Radushkevich etc. In the present work, four isotherms were studied quantitatively for each of the adsorbent used. The studies were carried out at optimum conditions by varying ARS concentrations from 50 to 500 mg L^{-1}.

Langmuir isotherm — The Langmuir isotherm model is used for monolayer adsorption on homogeneous surfaces. It accounts for the surface coverage by balancing the relative

rates of adsorption and desorption processes (Ayawei *et al.* 2015). The model assumes that there are finite numbers of adsorption sites available on the surface of the adsorbent that are identical and uniform in nature. Thus, once all the sites available are occupied by the adsorbate molecules, no further adsorption can take place. A saturation point is therefore achieved and maximum adsorption capacity can be easily calculated (Boparai *et al.* 2011). The linearized Langmuir equation can be represented as:

$$\frac{C_e}{q_e} = \frac{1}{q_{max}b} + \frac{C_e}{q_{max}} \tag{5}$$

where C_e is the equilibrium ARS concentration (mg L^{-1}), q_e is the amount of ARS adsorbed at equilibrium (mg g^{-1}), q_{max} is the adsorption capacity (mg g^{-1}) and b is a constant (L mg^{-1}) that shows the degree of interaction between ARS and the adsorbent surface. From the linear plots of C_e/q_e against C_e, the values of q_{max} and b can be calculated from the slope and intercept, respectively.

Freundlich isotherm — The Freundlich isotherm model is an empirical equation that describes the adsorption on inequivalent adsorption sites attributed to surface heterogeneity. It is applicable to both monolayer and multilayer adsorption phenomenon (Yang 1998). The linearized form of the Freundlich isotherm equation for aqueous solutions is given as:

$$\log q_e = \log K_F + \frac{1}{n}\log C_e \tag{6}$$

where K_F represents the Freundlich constant (mg g^{-1}) and n is the heterogeneity of the adsorbent surface and its affinity for the adsorbate (Chen *et al.* 2010). The significance of n is that it indicates the strength of the bond between adsorbate and adsorbent.

Halsey isotherm — The Halsey isotherm is used to evaluate multilayer adsorption at a relatively large distance from the surface (Ayawei *et al.* 2015). The linear form is expressed as:

$$q_e = \frac{1}{n_H}\ln K_H - \frac{1}{n_H}\ln C_e \tag{7}$$

where, K_H and n_H are Halsey isotherm constants that can be obtained from the values of slope and intercept of the plot of q_e versus $\ln C_e$.

Redlich–Peterson isotherm — The R–P isotherm is a mix of the Langmuir and Freundlich isotherms. It combines elements from both Langmuir and Freundlich equations; therefore, the mechanism is a mix and does not follow ideal monolayer adsorption (Brouers & Al-Musawi 2015). The linear form of the R–P isotherm is given as:

$$\ln\frac{C_e}{q_e} = \beta \ln C_e - \ln A \tag{8}$$

where A is the R–P isotherm constant (L g^{-1}) and β is the exponent that lies between 0 and 1. A plot of $\ln(C_e/q_e)$ verses $\ln C_e$ enables the determination of R–P constants.

The graphs for each of the adsorbent (Ch, SCC and SCC-B) showing the application of the above-mentioned isotherm models are provided in the supplementary materials (Supplementary Figures 2–4). The various constants associated with each of the above-mentioned isotherm models are listed in Table 1, along with the values of correlation coefficient.

From Table 1, it can be concluded that the Freundlich as well as the Halsey isotherm models were followed by all the adsorbents. Both of these models assume multilayer adsorption on heterogeneous adsorbent surface. The R–P isotherm also holds good for the adsorbents used. The R–P model is highly versatile because it can be used in both homogeneous and heterogeneous systems. The maximum adsorption capacity in accordance with the Langmuir isotherm was found to be 42.48 mg g^{-1} for the ARS-Ch system, 109.12 mg g^{-1} for the ARS-SCC system and 131.58 mg g^{-1} for the ARS-SCC-B system. These observations are in correlation with the SEM micrographs shown in Figure 2 and the BET surface area analysis. For native Ch, the adsorbent surface was found to be dense with a relatively lower surface

Table 1 | Summary of adsorption isotherms studied

Serial no.	Adsorption isotherms	Parameters	Adsorbents		
			Ch	SCC	SCC-B
1	Langmuir	K_L (L mg^{-1})	0.34	1.05	0.33
		q_{max} (mg g^{-1})	42.48	109.12	131.58
		R^2	0.9080	0.9681	0.9280
2	Freundlich	K_F (L mg^{-1})	1.88	4.73	1.62
		N	2.08	2.53	1.97
		R^2	0.9937	0.9912	0.9956
3	Halsey	K_H	3.71	50.88	2.58
		n_H	2.08	2.53	1.97
		R^2	0.9937	0.9912	0.9956
4	Redlich–Peterson (R–P)	B	0.52	0.60	0.49
		A (L g^{-1})	0.53	0.21	0.62
		R^2	0.9946	0.9962	0.9953

area. The morphology was found to become more folded in SSC. However, the surface area was found to decrease due to the cross-linking phenomenon. The adsorption capacity was found to increase due to the fact that cross-linking leads to trapping of dye molecules (Jeyaseelan *et al.* 2018) for SCC-B, the morphology became more porous with bentonite–Ch composite formation. This led to an increased surface area and an increased adsorption capacity.

Kinetic studies

In order to understand the mechanism of the adsorption process, two kinetic models, namely pseudo-first-order and pseudo-second-order, were used. The best-fit model was assessed on the basis of the value of linear coefficient of determination (R^2). In order to check if diffusion process was involved, the Weber–Morris model of intra-particle diffusion was studied (Figure 8). These studies were carried out at optimized values of all parameters for the adsorbent applied.

The pseudo-first-order model is used to describe the reversibility of the equilibrium between liquid and solid phases based on the sorption capacity of solids (Ho 2004). It is expected that one sorption site on the surface of the adsorbent is occupied by a single adsorbate molecule. The linear form of rate expression of Lagergren for pseudo-first-order model (Ho 2004) is given as:

$$\log(q_e - q_t) = \log q_e - \frac{tk_1}{2.303} \tag{9}$$

where q_e and q_t refers to the amount of dye adsorbed (mg g^{-1}) at equilibrium and at time t (min), and k_1 is the first-order rate constant (min^{-1}) of the pseudo-first-order process. The linear plots (Supplementary Figure 5a, 5c and 5e, respectively for Ch, SCC and SCC-B adsorbents) of $\log(q_e - q_t)$ against t are useful to predict the rate constant k_1 and adsorption at equilibrium (mg g^{-}) from the values of slope and intercept, respectively.

The pseudo-second-order equation assumes that the rate-limiting step might be due to the chemical adsorption (Ho & McKay 2000; Ho 2004; Ho 2006) and involves the prediction that one adsorbate molecule occupies two distinct sorption sites available on the surface of the adsorbent. The rate expression is given as:

$$\frac{t}{q_t} = \frac{1}{k_2 q_e^2} + \frac{t}{q_e} \tag{10}$$

where, k_2 is the pseudo-second-order rate constant (g mg^{-1} min^{-1}), and the equilibrium adsorption capacity q_e can be calculated from the slope and intercept value obtained from the plot (Supplementary Figure 5b, 5d and 5f, respectively, for Ch, SCC and SCC-B adsorbents) of t/q_t against t.

During adsorption, whether intra-particle diffusion is the rate determining step can be confirmed by the Weber–Morris model (Weber & Morris 1964). According to this model, q_t and $t^{1/2}$ of the adsorption process are related as:

$$q_t = k_{int} \cdot t^{\frac{1}{2}} + C \tag{11}$$

where k_{int} is the rate constant (mg g^{-1} $min^{1/2}$) of the diffusion process and C is a constant that gives an idea about the thickness of the boundary layer, i.e. the larger the value of C, the greater the boundary layer effect. If the plot of q_t verses $t^{1/2}$ passes through the origin and is linear, then intra-particle diffusion is the only rate-limiting step.

Regarding the suitability of pseudo-first-order model, it is evident from the values of R^2 and the poor agreement between the q_e (exp) and q_e (cal) values that it is not the

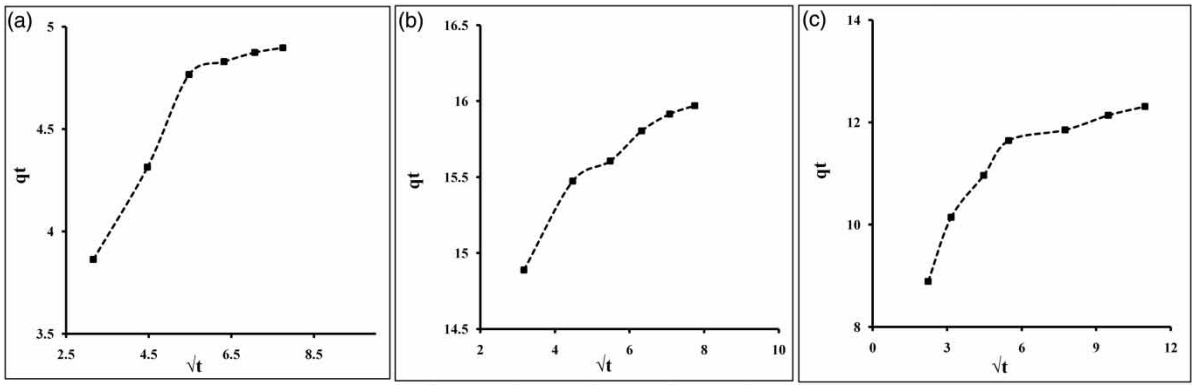

Figure 8 | Intra-particle diffusion model for (a) Ch (b) SCC and (c) SCC-B adsorbents.

Table 2 | Adsorption kinetic models for the adsorption of ARS dye

		Pseudo-first-order			Pseudo-second-order			Intra-particle diffusion	
Adsorbent	Q_e (exp)	k_1 (min^{-1})	q_e (cal)	R^2	k_2 (mg g^{-1} min^{-1})	q_e (cal)	R^2	k_{int} (mg g^{-1} min$^{-1/2}$)	R^2
Ch	4.5208	0.0915	2.7542	0.9153	0.0551	5.2110	1.0000	0.2293	0.8744
SCC	11.6959	0.0040	3.2449	0.8792	0.0622	16.2074	1.0000	0.2270	0.9285
SCC-B	11.2000	0.0341	4.8978	0.9586	0.0323	12.5000	0.9999	0.3395	0.8051

best-fit model (Table 2). On the contrary, the R^2 values obtained by pseudo-second-order model were 1.00 fit in case of all three adsorbents. The q_e (exp) and q_e (cal) were also in close association compared to the former model. This suggests that the pseudo-second-order model is best-fit for all three adsorbents.

Adsorption mechanism

It has been suggested that the overall rate of adsorption can be described by the following three steps (Boparai *et al.* 2011; Chingombe *et al.* 2006): (1) film or surface diffusion, where the sorbate is transported from the bulk solution to the external surface of sorbent, (2) intra-particle or pore diffusion, where sorbate molecules move into the interior of sorbent particles and (3) adsorption on the interior sites of the sorbent. Since the adsorption step is very rapid, it is assumed that it does not influence the overall kinetics. The overall rate of adsorption process, therefore, will be controlled by either surface diffusion or intra-particle diffusion. The Weber–Morris intra-particle diffusion model (Figure 8) has often been used to determine if intra-particle diffusion is the rate-limiting step (Kavitha & Namasivayam 2007; Taqvi *et al.* 2007; Wu *et al.* 2009).

As suggested by Ozcan *et al.* (2007) in his work, a plot of q_t versus $t^{1/2}$ should be linear if intra-particle diffusion is involved in the adsorption process, and if the plot passes through the origin then intra-particle diffusion is the only rate-limiting step. It has also been suggested that in instances when q_t versus $t^{0.5}$ is multi-linear, two or more steps govern the adsorption process (Unuabonah *et al.* 2007; Wu *et al.* 2009). The initial steeper section represents surface or film diffusion, the second linear section represents a gradual adsorption stage where intra-particle or pore diffusion is rate-limiting and the third section is the final equilibrium stage. As the plot did not pass through the origin, intra-particle diffusion was not the only rate-limiting step. Thus, apart from intra-particle diffusion, some degree of boundary layer diffusion also affected the adsorption process.

Adsorption thermodynamics

The effect of temperature on the adsorption process of ARS with different adsorbents was studied to obtain the thermodynamic parameters that decide the spontaneity and feasibility of the process. These parameters can be easily determined from the thermodynamic equilibrium constant, K.

The free energy change accompanying the process is calculated as:

$$\Delta G = -RT \ln K \tag{12}$$

The entropy and enthalpy changes were determined using van 't Hoff equation as follows:

$$\ln K = (\Delta S/R) - (\Delta H/RT) \tag{13}$$

where R is the gas constant (8.314 J mol^{-1} K^{-1}) and T is the absolute temperature (K). The equilibrium constant K_L was obtained from the ratio of ARS on the adsorbent to that in the solution phase. The values of ΔH and ΔS are obtained from the graph of lnK_L verses $1/T$ (Supplementary Figure 6).

With reference to Table 3, the negative values of ΔG for all three adsorbents indicate that the process of adsorption of ARS is spontaneous in nature. The negative values of ΔH for all three adsorbents shows that the process is exothermic and the negative values of ΔS indicates that the randomness in the moieties is decreasing as adsorption of dyes on the surface of the adsorbent molecules progresses. As can be seen from Table 3, as the temperature increases from 303 to 333 K, the ΔG values become less negative, indicating that adsorption capacity decreases with an increase in temperature.

Column studies

Adsorption using column is one of the most common and efficient way for removal of pollutants from water (Gupta *et al.* 2016). However, it is worth noting that it may be helpful that before evaluating the feat of adsorbent in a fixed-bed

Table 3 | Adsorption thermodynamics of adsorption of ARS dye

Serial no.	Adsorbent	Parameters	Temperatures (K)			
			303	313	323	333
1	Ch	ΔG (kJ mol^{-1})	−7.53	−6.79	−6.05	−5.31
		ΔH (kJ mol^{-1})	− 29.95			
		ΔS (J mol^{-1} K^{-1})	− 74			
2	SCC	ΔG (kJ mol^{-1})	−6.49	−6.19	−5.89	−5.59
		ΔH (kJ mol^{-1})	− 15.58			
		ΔS (J mol^{-1} K^{-1})	− 30.2			
3	SCC-B	ΔG (kJ mol^{-1})	−11.75	−9.90	−8.05	−6.20
		ΔH (kJ mol^{-1})	− 67.81			
		ΔS (J mol^{-1} K^{-1})	− 185			

adsorber, adsorption isotherm studies such as batch experiments were conducted to calculate the maximum adsorption capacity of the adsorbent (Al-Degs *et al.* 2009). Columns have an advantage over batch because a continuous flow is maintained over a fixed-bed, thereby increasing the adsorbent capacity, which is contrary to batch where the concentration gradient between adsorbent and adsorbate decreases with time (Anderson *et al.* 2012). A plot of C_C/C_o against volume of ARS solution (Supplementary Figure 7) eluted was plotted to determine the values of various column parameters.

It can be observed from Table 4 that the exhaustion capacities of all three materials are higher than adsorption capacities obtained in batch studies. Due to this, larger sample volumes (exhaustion volume) can be treated with column compared to batch studies.

CONCLUSION

ARS is a potent water pollutant. Three adsorbents, namely Ch, SCC and SCC-B were used for the removal of ARS using batch and column adsorption methods. All adsorbents were extensively characterized using various spectral techniques, such as FT-IR, SEM, EDX, XRD, BET and TGA-DTA analysis, to confirm the nature and presence of different active sites. Parameters such as pH_{PZC} of adsorbent, pH of dye solution, contact time, adsorbent dose and temperature were optimized to obtain a maximum removal efficiency. Four adsorption isotherms models were studied, namely Langmuir, Freundlich, Halsey, and R–P. Maximum adsorption capacity was found to be 42.48 mg g^{-1} for Ch, 109.12 mg g^{-1} for SCC and 131.58 mg g^{-1} for SCC-B. This was the expected result because the introduction of new groups impart newer active sites on the surface of the polymer, which leads to binding of large numbers of dye molecules. For SCC-B, the surface is modified by both cross-linking by sulphate group and physical adherence of clay molecules, and hence it showed good adsorption properties with maximum removal capacity. Adsorption kinetics was best-fitted with the pseudo-second-order model and showed high correlation coefficients, $R^2 \geq 0.9999$ for all the three adsorbents. An intra-particle diffusion model was also studied to determine the course of adsorption and its

Table 4 | Column parameters for the adsorption of ARS dye

Serial no.	Parameters	ARS with Ch	ARS with SCC	ARS with SCC-B
1	Weight of adsorbent (g)	1.00	1.00	1.00
2	Initial dye concentration (mg L^{-1})	50	50	50
3	Flow rate (mL min^{-1})	5.0	5.0	5.0
4	Breakthrough volume (mL)	450	950	2,100
5	Exhaustion volume (mL)	1,350	2,900	3,750
6	Breakthrough capacity (mg g^{-1})	22.5	47.5	105
7	Exhaustion capacity (mg g^{-1})	67.5	145	187.5
8	Degree of column utilization (%)	33.33	32.76	56.00

Table 5 | Comparison of Ch, SCC and SCC-B with other materials for ARS adsorption

Serial no.	Material	Adsorption capacity (mg g^{-1})	Reference
1	Magnetic chitosan	40.12	Fan *et al.* (2011)
2	Chitosan beads (CS)	133.33	Omnia & Sahar (2017)
3	Chitosan/ZnO nanorod composite (CS-ZnO)	111.11	Omnia & Sahar (2017)
4	Activated clay modified by iron oxide (Fe-clay)	32.7	Fu *et al.* (2011)
5	Graphene oxide (GO)	88.50	Nuengmatcha *et al.* (2016)
6	Bare graphite powder (BGP)	34.13	Nuengmatcha *et al.* (2016)
7	Polyvinyl alcohol-alginate bound nano magnetite microspheres modified with cetyltrimethyl ammonium bromide (PVAANM/CTAB)	118.6	Tiwari & Kathane (2017)
8	Termite hill sample (THs)	1.425	Ayanda *et al.* (2019)
9	Chitosan	42.48	Present study
10	SCC	109.12	Present study
11	SCC-B	131.58	Present study

mechanism. Adsorption thermodynamics showed that the process occurs spontaneously, as shown by the negative values of change in free energy with release of heat (exothermic). Column studies were also carried out to evaluate the column parameters. From the values of exhaustion capacity, it was found that the column adsorption method is more suitable for large sample volumes compared to the batch adsorption method. A comparison of these three materials with other materials towards removal of ARS is presented in Table 5. It is clear from the table that SCC and SCC-B are excellent adsorbents for ARS, with higher adsorption capacities compared to most of Ch-based materials reported in literature.

ACKNOWLEDGEMENT

The authors are thankful to RTM Nagpur University, Nagpur and PG Department of Chemistry for providing all the necessary facilities for the research work. Special thanks to Dr S. Kahu and Dr A. Shekhawat for helping in calculation work, writing style and proofreading.

FUNDING

This work was supported by Department of Science and Technology (DST), New Delhi under the DST INSPIRE Fellowship Program [Sanction order no. DST/INSPIRE Fellowship/2017/IF170496 dated 16 July 2019] and RTM Nagpur University under University Research Scheme.

DATA AVAILABILITY STATEMENT

All relevant data are included in the paper or its Supplementary Information.

REFERENCES

Adekola, F. A. & Adegoke, H. I. 2005 Adsorption of blue-dye on activated carbons produced from rice husk, coconut shell and coconut coir pith. *Ife Journal of Science* **7**, 151–157. http://dx.doi.org/10.4314/ijs.v7i1.32169.

Adeyemo, A., Adeoye, I. & Bello, O. 2017 Adsorption of dyes using different types of clay: a review. *Applied Water Science* **7**, 543–568. https://doi.org/10.1007/s13201-015-0322-y.

Al-Degs, Y., Khraisheh, M., Allen, S. & Ahmad, M. 2009 Adsorption characteristics of reactive dyes in columns of activated carbon. *Journal of Hazardous Materials* **165** (1–3), 944–949. http://doi.org/10.1016/j.jhazmat.2008.10.081.

Andersson, K., Eriksson, M. & Norgren, M. 2012 Lignin removal by adsorption to fly ash in wastewater generated by mechanical pulping. *Industrial & Engineering Chemistry Research* **51** (8), 3444–3451. https://doi.org/10.1021/ie202462z.

Anirudhan, T. S., Rijith, S. & Tharun, A. R. 2010 Adsorptive removal of thorium (IV) from aqueous solutions using

poly(methacrylic acid)-grafted chitosan/bentonite composite matrix: process design and equilibrium studies. *Colloids and Surfaces A: Physicochemical and Engineering Aspects* **368**, 13–22. https://doi.org/10.1016/j.colsurfa.2010.07.005.

Ayanda, O., Amodu, O., Adubiaro, H., Olutona, G., Ebenezer, O., Nelana, S. & Naidoo, E. 2019 Effectiveness of termite hill as an economic adsorbent for the adsorption of alizarin red dye. *Journal of Water Reuse and Desalination* **9**, 83–93. https://doi.org/10.2166/wrd.2018.026.

Ayawei, N., Ekubo, A. T., Wankasi, D. & Dikio, E. D. 2015 Adsorption of Congo red by Ni/Al-CO_3: equilibrium, thermodynamics and kinetic studies. *Oriental Journal of Chemistry* **31**, 1307–1318. http://dx.doi.org/10.13005/ojc/310307.

Azzeddine, E. R. & Abdelali, I. 2014 Physico-chemical and mineralogical characterization of a Moroccan bentonite (Azzouzet) and determination of its nature and its chemical structure. *International Journal of Materials Science and Applications* **3**, 42–48. https://doi:10.11648/j.ijmsa.20140302.16.

Bellir, K., Bencheikh-Lehocine, M. & Meniai, A. H. 2010 Removal of methylene blue from aqueous solutions using an acid activated Algerian bentonite: equilibrium and kinetic studies. *Applied Clay Science* **153**, 38–45. http://dx.doi.org/10.1016/j.clay.2017.11.034.

Bharathi, K. S. & Ramesh, S. T. 2013 Removal of dyes using agricultural waste as low-cost adsorbents: a review. *Applied Water Science* **3**, 773–790. https://doi.org/10.1007/s13201-013-0117-y.

Boparai, H., Joseph, M. & O'Carroll, D. 2011 Kinetics and thermodynamics of cadmium ion removal by adsorption onto nano zerovalent iron particles. *Journal of Hazardous Materials* **186**, 458–465. https://doi.org/10.1016/j.jhazmat.2010.11.029.

Brouers, F. & Al-Musawi, T. J. 2015 On the optimal use of isotherm models for the characterization of bio sorption of lead onto algae. *Journal of Molecular Liquids* **212**, 46–51. https://doi.org/10.1016/j.molliq.2015.08.054.

Bulut, Y. & Aydin, H. 2006 A kinetics and thermodynamics study of methylene blue adsorption on wheat shells. *Desalination* **194**, 259–267. https://doi.org/10.1016/j.desal.2005.10.032.

Chatterjee, S., Chatterjee, S., Chatterjee, B. & Guha, A. 2007 Adsorptive removal of Congo red, a carcinogenic textile dye by chitosan hydro beads: binding mechanism, equilibrium and kinetics. *Colloids and Surfaces A: Physicochemical and Engineering Aspects* **299**, 146–152. https://doi.org/10.1016/j.colsurfa.2006.11.036.

Chen, H. & Zhao, J. 2009 Adsorption study for removal of Congo red anionic dye using organ-attapulgite. *Adsorption* **15**, 381–389. https://doi.org/10.1007/s10450-009-9155-z.

Chen, S., Zhang, J., Zhang, C., Yue, Q., Li, Y. & Li, C. 2010 Equilibrium and kinetic studies of methyl orange and methyl violet adsorption on activated carbon derived from *Phragmites australis*. *Desalination* **252**, 149–156. https://doi.org/10.1016/j.desal.2009.10.010.

Chingombe, P., Saha, B. & Wakeman, R. 2006 Sorption of atrazine on conventional and surface modified activated carbons. *Journal of Colloid and Interface Science* **302**, 408–416. https://doi.org/10.1016/j.jcis.2006.06.065.

Crini, G. 2006 Non-conventional low-cost adsorbents for dye removal: a review. *Bioresource Technology* **97**, 1061–1085. https://doi.org/10.1016/j.biortech.2005.05.001.

Dotto, G. L., Rodrigues, F. K., Tanabe, E. H., Frohlich, R., Bertuol, D. A., Martins, T. R. & Foletto, E. L. 2016 Development of chitosan/bentonite hybrid composite to remove hazardous anionic and cationic dyes from colored effluents. *Journal of Environmental Chemical Engineering* **4**, 3230–3239. http://doi.org/10.1016/j.jece.2016.07.004.

Fan, L., Zhang, Y., Li, X., Luo, C., Lu, F. & Qiu, H. 2011 Removal of alizarin red from water environment using magnetic chitosan with Alizarin Red as imprinted molecules. colloids and surfaces. B. *Biointerfaces* **91**, 250–257. 10.1016/j.colsurfb.2011.11.014.

Fu, F., Gao, Z., Gao, L. & Li, D. 2011 Effective adsorption of anionic dye, alizarin Red S, from aqueous solutions on activated clay modified by iron oxide. *Industrial & Engineering Chemistry Research* **50**, 9712–9717. https://dx.doi.org/10.1021/ie200524b.

Grozdanov, A., Atkovska, K., Bliznakovska, B., Ruseska, G., Bogoevski, S. & Boskovski, B. 2016 Adsorption of Fe(II) and Zn(II) ions from landfill leachate by natural bentonite. *Journal of Chemical Technology & Metallurgy* **51** (2), 215–222. https://www.researchgate.net/publication/298353654.

Gupta, V. K., Suhas, T. I., Agarwal, S., Singh, R., Chaudhary, M., Harit, A. & Kushwaha, S. 2016 Column operation studies for the removal of dyes and phenols using a low cost adsorbent. *Global Journal of Environmental Science and Management* **2** (1), 1–10. https://doi.org/10.7508/gjesm.2016.01.001.

Ho, Y. S. 2004 Citation review of Lagergren kinetic rate equation on adsorption reactions. *Scientometrics* **59**, 171–177. https://doi.org/10.1023/B:SCIE.0000013305.99473.cf.

Ho, Y. S. 2006 Review of second-order models for adsorption systems. *Journal of Hazardous Materials* **136**, 681–689. http://doi.org/10.1016/j.jhazmat.2005.12.043.

Ho, Y. & Ching, C. 2001 Sorption studies of acid dye by mixed sorbents. *Adsorption* **7**, 139–147. https://doi.org/10.1023/A:1011652224816.

Ho, Y. S. & McKay, G. 2000 The kinetics of divalent metal ions onto sphagnum moss peat. *Water Research* **34**, 735–742. https://doi.org/10.1016/S0043-1354(99)00232-8.

Holmgren, A., Forsling, W. & Wu, L. 1997 An FT-IR study of Alizarin Red S adsorbed at the fluorapatite-water interface. *Progress in Fourier Transform Spectroscopy* **14**, 197–199. urn:nbn:se:ltu:diva-14864.

Huang, R., Liu, Q., Zhang, L. & Yang, B. 2015 Utilization of cross-linked chitosan/bentonite composite in the removal of methyl orange aqueous solution. *Water Science and Technology* **71** (2), 174–182. https://doi.org/10.2166/wst.2014.478.

Huang, R., Zhang, L., Hu, P. & Wang, J. 2016 Adsorptive removal of Congo red from aqueous solutions using cross-linked chitosan and cross-linked chitosan immobilized bentonite. *International Journal of Biological Macromolecules*. http://dx.doi.org/doi:10.1016/j.ijbiomac.2016.01.083.

Jeyaseelan, C., Chaudhary, N. & Jugade, R. 2018 Sulphate-crosslinked chitosan as an adsorbent for the removal of Congo red dye from

aqueous solution. *Air, Soil and Water Research (ASW)* **11**, 1–8. https://doi.org/10.1177/1178622118811680.

Kahu, S., Saravanan, D. & Jugade, R. 2014 Effective detoxification of hexavalent chromium using sulfate cross-linked chitosan. *Water Science and Technology* **9**, 1091–1100. https://doi.org/10.2166/wst.2014.455.

Kavitha, D. & Namasivayam, C. 2007 Experimental and kinetic studies on methylene blue adsorption by coir pith carbon. *Bioresource Technology* **98**, 14–21. https://doi.org/10.1016/j.biortech.2005.12.008.

Komosińska, J., Dulewska, C., Pająk, M., Krzyżewska, I. & Dzieniszewska, A. 2014 Adsorption of anionic dyes onto natural, thermally and chemically modified smectite clays. *Polish Journal of Chemical Technology (PJCT)* **16**, 33–40. https://doi.org/10.2478/pjct-2014-0066.

Kyzas, G. Z. & Bikiaris, D. N. 2015 Recent modifications of chitosan for adsorption applications: a critical and systematic review. *Marine Drugs* **13**, 312–337. https://doi.org/10.3390/md13010312.

Kyzioł-Komosińska, J., Rosik-Dulewska, C., Pająk, M., Krzyżewska, I. & Dzieniszewska, A. 2014 Adsorption of anionic dyes onto natural, thermally and chemically modified smectite clays. *Polish Journal of Chemical Technology* **16**, 33–40. https://doi.org/10.2478/pjct-2014-0066.

Mahmoodi, N. M., Hayati, B., Arami, M. & Lan, C. 2011 Adsorption of textile dyes on pine cone from colored wastewater: kinetic, equilibrium and thermodynamic studies. *Desalination* **268**, 117–125. https://doi.org/10.1016/j.desal.2010.10.007.

Nair, V., Panigrahy, A. & Vinu, R. 2014 Development of novel chitosan-lignin composites for adsorption of dyes and metal ions from wastewater. *Journal of Chemical Engineering* **254**, 491–502. https://doi.org/10.1016/j.cej.2014.05.045.

Namasivayam, C. & Kavitha, D. 2002 Removal of Congo red from water by adsorption on to activated carbon prepared from coir pith, an agricultural solid waste. *Dyes and Pigments* **54**, 47–58. https://doi.org/10.1016/S0143-7208(02)00025-6.

Naushad, M., Sharma, G. & Alothman, Z. 2019 Photodegradation of toxic dye using Gum Arabic-crosslinked-poly(acrylamide)/Ni(OH)2/FeOOH nanocomposites hydrogel. *Journal of Cleaner Production* **241**, 1–9. https://doi.org/10.1016/j.jclepro.2019.118263.

Nesic, A. R., Velickovic, S. J. & Antonovic, D. G. 2013 Modification of chitosan by zeolite A and adsorption of bezactive orange 16 from aqueous solution. *Composites Part B: Engineering* **53**, 145–151. https://doi.org/10.1016/j.compositesb.2013.04.053.

Nuengmatcha, P., Mahachai, R. & Chanthai, S. 2016 Adsorption capacity of the as-synthetic graphene oxide for the removal of alizarin red S dye from aqueous solution. *Oriental Journal of Chemistry* **32**, 1399–1410. http://dx.doi.org/10.13005/ojc/320314.

Omnia, A. & Sahar, M. 2017 Adsorption of copper ions and alizarin red S from aqueous solutions onto a polymeric nanocomposite in single and binary systems. *Turkish Journal of Chemistry* **41**, 967–986. https://doi.org/10.3906/kim-1703-72.

Ozcan, A., Ozcan, A. S. & Gok, O. 2007 Adsorption kinetics and isotherms of anionic dye of reactive blue 19 from aqueous solutions onto DTMA-sepiolite. In: *Hazardous Materials and Wastewater – Treatment, Removal and Analysis* (A. A. Lewinsky, ed.). Nova Science Publishers, New York.

Saha, T. K., Bhoumik, N. C., Karmaker, S., Ahmed, M. G., Ichikawa, H. & Fukumori, Y. 2010 Adsorption of methyl orange onto chitosan from aqueous solution. *Journal of Water Resource and Protection (JWARP)* **2**, 898–906. https://doi.org/10.4236/jwarp.2010.210107.

Salleh, M. A. M., Mahmoud, D. K., Karim, W. A. W. A. & Idris, A. 2011 Cationic and anionic dye adsorption by agricultural solid waste: a comprehensive review. *Desalination* **280**, 1–13. https://doi.org/10.1016/j.desal.2011.07.019.

Saravanan, D., Gomathi, T. & Sudha, P. N. 2013 Sorption studies on heavy metal removal using chitin/bentonite biocomposite. *International Journal of Biological Macromolecules* **53**, 67–71. https://doi.org/10.1016/j.ijbiomac.2012.11.005.

Savitri, E. & Budhyantaro, A. 2017 The effect of ratio chitosan-bentonite and processing time on the characterization of chitosan-bentonite composite. *IOP Conference Series Materials Science and Engineering* **223**, 1–8. https://doi.org/10.1088/1757-899X/223/1/012034.

Shekhawat, A., Kahu, S., Saravanan, D. & Jugade, R. 2015 Synergistic behaviour of ionic liquid impregnated sulphate-crosslinked chitosan towards adsorption of Cr(VI). *International Journal of Biological Macromolecules* **80**, 615–626. https://doi.org/10.1016/j.ijbiomac.2015.07.035.

Singh, K. P., Mohan, D., Sinha, S., Tondon, G. S. & Gosh, D. 2003 Color removal from wastewater using low-cost activated carbon derived from agricultural waste material. *Industrial & Engineering Chemistry Research* **42**, 1965–1976. https://doi.org/10.1021/ie020800d.

Taqvi, S. I. H., Hasany, S. & Bhanger, M. 2007 Sorption profile of Cd(II) ions onto beach sand from aqueous solutions. *Journal of Hazardous Materials* **141**, 37–44. https://doi.org/10.1016/j.jhazmat.2006.06.080.

Tiwari, A. & Kathane, P. 2017 Effective removal of dye alizarin Red S using CTAB modified PVA-Alginate bound nano magnetite microspheres. *International Journal of Scientific and Technical Research in Engineering* **2**, 33–41.

Tripathy, S., Bersillon, J. & Gopal, K. 2006 Removal of fluoride from drinking water by adsorption onto alum-impregnated activated alumina. *Separation and Purification Technology* **50**, 310–317. https://doi.org/10.1016/j.seppur.2005.11.036.

Unuabonah, E., Adebowale, K. & Olu-Owolabi, B. 2007 Kinetic and thermodynamic studies of the adsorption of lead(II) ions onto phosphate-modified kaolinite clay. *Journal of Hazardous Materials* **144**, 386–395.

Vital, R. K., Saibaba, K. V. N., Shaik, K. B. & Gopinath, R. 2016 Dye removal by adsorption: a review. *Journal of Bioremediation & Biodegradation* **7**, 371. https://doi.org/10.4172/2155-6199.1000371.

Weber, W. J. & Morris, J. C. 1964 Equilibria and capacities for adsorption on carbon. *Journal of the Sanitary Engineering Division* **90**, 79–108.

Wu, F., Tseng, R. & Juang, R. 2009 Initial behavior of intraparticle diffusion model used in the description of adsorption

kinetics. *Chemical Engineering Journal* **153**, 1–8. https://doi.org/10.1016/j.cej.2009.04.042.

Yang, C. 1998 Statistical mechanical study on the Freundlich isotherm equation. *Journal of Colloid and Interface Science* **208**, 379–387. https://doi.org/10.1006/jcis.1998.5843.

Zhang, L., Hu, P., Wang, J. & Huang, R. 2016 Crosslinked quaternized chitosan/bentonite composite for the removal of Amino black 10B from aqueous solutions. *International Journal of Biological Macromolecules*. http://dx.doi.org/10.1016/j.ijbiomac.2016.08.018.

First received 22 June 2020; accepted in revised form 28 July 2020. Available online 10 August 2020